ELSEVIER

Biophysical Chemistry 134 (2008) 168–177

Biophysical Chemistry

http://www.elsevier.com/locate/biophyschem

Lipid membrane domain formation and alamethicin aggregation studied by calorimetry, sound velocity measurements, and atomic force microscopy

Vitaliy Oliynyk [a,b], Markus Jäger [a], Thomas Heimburg [b], Vitaly Buckin [c], Udo Kaatze [a,*]

[a] *Complex Fluids Group, Drittes Physikalisches Institut, Georg-August-Universität, Friedrich-Hund-Platz 1, D-37077 Göttingen, Germany*
[b] *Membrane Biophysics Group, Niels Bohr Institute, University of Copenhagen, Blegdamsvej 17, DK-2100 Copenhagen Ø, Denmark*
[c] *School of Chemistry & Chemical Biology, University College Dublin, Dublin 4, Ireland*

Received 15 November 2007; received in revised form 7 February 2008; accepted 9 February 2008
Available online 10 March 2008

Abstract

An experimental study of phosphocholine membranes made from one lipid, from mixtures of DPPC and DLPC, and also from lipids and small amounts of alamethicin is presented. We used atomic force microscopy to investigate the spatial organization and structure of lipid domains and also of the defects induced by the peptide. Alamethicin was found to alter the state of lipids in the gel state in a way that domains of fluid lipids are formed close to the defects. Differential calorimetry revealed phase characteristics of the lipid mixtures and the effect of small amounts of alamethicin on the phase behavior. It was also shown that the sound velocity profiles of the membranes suspensions can be well calculated from the heat capacity traces of the samples. This result confirms the correlation between the mechanical properties and the specific heat of membrane systems.

Keywords: Lipid membranes; Alamethicin; Peptide pores; Atomic force microscopy; Sound velocity; Differential scanning calorimetry

1. Introduction

Membranes play a significant role in the organization and function of living systems [1,2]. For this reason much attention has been directed towards phospholipid bilayers which are widely accepted as models for biological membranes. In particular, the main phase transition, at which the bilayers change their properties substantially, has been the focus of continuous scientific interest. It appears that this phase transition from a solid-like ordered (gel) phase to a liquid-like disordered (fluid) phase occurs in the vicinity of a critical point. Near the phase transition temperature T_m, bilayer structures display thermodynamic fluctuations over wide ranges of length scales. These fluctuations are considered essential for biological functions [3,4]. The gel–fluid transition is from a phase with crystalline lateral packing (solid) to a phase without crystalline order (liquid). The transition regime is characterized by fluctuations in lipid state leading to domain formation. In the literature a related transition is often discussed in the context of micro-domain formation in biological membranes called 'rafts'. This is the transition from liquid-ordered (lo) to liquid-disordered (ld). The low temperature states of both transitions display ordered chains and thus low enthalpy. In practice, it may often be difficult to distinguish these two transitions in experiment. Both transition events are accompanied by heat capacity anomalies on which much of the below argument is based. For this reason, the (lo) to (ld) transition has recently also been related to critical fluctuations [5]. Thus, much of what is discussed below may also be correct for the (lo) to (ld) transition.

In the temperature range around T_m a one-compound lipid bilayer exhibits a distribution of domains of molecules with conformationally disordered chains in a conformationally ordered phase and vice versa [6,7]. The size of the individual lipid domain is an equilibrium property [8] that scales with inverse reduced temperature $\epsilon^{-1} = T_m/|T - T_m|$. It has been suggested that any membrane process, proceeding on length scales smaller than or on the order of the domain size, is controlled by the fluctuations so

* Corresponding author. Tel.: +49 551 39 7715; fax: +49 551 39 7720.
E-mail address: uka@physik3.gwdg.de (U. Kaatze).

0301-4622/$ - see front matter © 2008 Elsevier B.V. All rights reserved.
doi:10.1016/j.bpc.2008.02.004

that the domain structure affects the biological functions associated with membranes. The effect of temperature upon the dynamics of domain structure fluctuations may be visualized by the substantial enhancement in the relaxation time τ_ξ near T_m [9,10] which, for a 1,2-dimyristoyl-3-*sn*-phosphocholine vesicle solution in water, is shown in Fig. 1. By analogy with the dynamic scaling hypothesis of critical phenomena [11–13] τ_ξ is the characteristic time scale correlated with the size parameter describing the domains. Hence the slowing in the fluctuations near T_m (Fig. 1) reflects the strongly increasing average domain size when approaching the phase transition temperature. Because of the effect of domain structure fluctuations on the biological functions associated with membranes, it is interesting to gain deeper insights into the lateral dimensions of the domain and into their influence on thermodynamic and mechanical membrane properties. As a matter of fact one finds relaxation processes on many time scales from pico-seconds to minutes. However, the fastest fluctuations can even be attributed to events below the molecular scale, like *trans–gauche* isomerizations of chains. Domain formation makes up for at least 90% of the total heat and thus is responsible for most of the excess heat capacity. Therefore, most of the fluctuations in volume and heat can be attributed to the large scale cooperative processes [14,15].

Biological membranes are composed of a large number of different lipids and a variety of proteins, leading to dynamically highly microheterogeneous structure. Due to the interactions between the constituents various types of domains and subdomains may be formed. The structural complexity following thereby likely contributes to the activity of a large number of membrane-associated biochemical processes. On the other hand, however, it awfully complicates the deduction of detailed physical conclusions from investigations of native membranes. We thus found it interesting to study simplified model systems, namely mixtures of phospholipids with different acyl chain lengths and also alamethicin-containing lipid membranes.

The membrane active peptide alamethicin, isolated from the fungus *Trichoderma viride*, is among the most intensively studied peptides [16,17]. Its amino-acid sequence, its crystal structure,

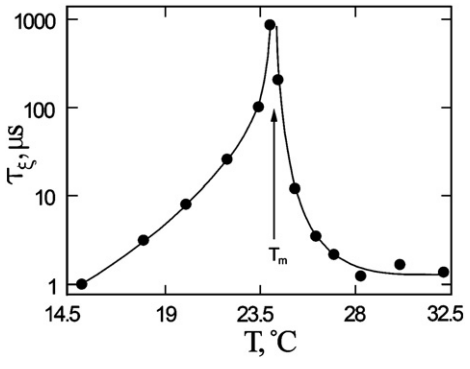

Fig. 1. Relaxation time τ_ξ of domain structure fluctuations of aqueous solutions of extruded vesicles from 1,2-dimyristoyl-*sn*-glycero-3-phosphocholine versus temperature T near the phase transition temperature T_m. τ_ξ values have been derived from an evaluation of broadband (100 kHz to 2 GHz) ultrasonic attenuation spectra [9,10] using theoretical arguments [9] to show the suitability of the Bhattacharjee–Ferrell dynamic scaling theory [65–67] which had been originally derived to apply for critical concentration fluctuations of binary fluids.

and its helical structure in water as well as in membrane is well known [1,18]. Alamethicin is among the antibiotic peptides serving as membrane permeating agents in host defense systems of organisms. At low peptide-to-lipid molar ratios (P/L) alamethicin preferentially adsorbs to the membrane surface where it is aligned in parallel to the lipid head groups. Above a certain concentration nearly all peptide molecules participate in the formation of pores, constituting mildly cation-selective ion channels [19–23]. As the channel activity shows discrete multilevel conductances [24–26], a barrel stave model has been suggested for the channels. Within the framework of this model the discrete conductance steps are assumed to result from a varying number of pore-forming helical alamethicin molecules arranged to form a water-filled channel [27,28]. There exists strong evidence that the effect of such integral peptides on the phase characteristics of lipid membranes strongly depends on the length of lipid acyl chains [29]. It is assumed that the hydrophobic mismatch, due to the relative lengths difference between the peptide and lipid hydrocarbon parts, plays a significant role in the structure of membranes [30,31].

In this article we study structural and elastic properties of mixed phospholipid membranes as well as alamethicin-containing bilayer membranes by using atomic force microscopy (AFM). We also present sound velocity, density and calorimetric data to demonstrate the correlation between compressibility, heat capacity and the AFM images. The goal is to show the relation between the thermodynamic properties of peptide-containing membranes with the lateral arrangement of peptides and lipids. This implies a coupling between the arrangement of molecules and their elastic behavior.

2. Materials and methods

1,2-dipalmitoyl-*sn*-glycero-3-phosphatidylcholine (DPPC), 1,2-dimyristoyl-*sn*-glycero-3-phosphatidylcholine (DMPC) and 1,2-dilauroyl-*sn*-glycero-3-phosphocholine (DLPC) were purchased from Avanti Polar Lipids (Alabaster, AL, USA), Fluka, and Sigma (both Taufkirchen, FRG). Alamethicin was also provided by Sigma. All substances were used without additional purification. Ruby muscovite mica was obtained from TED PELLA, inc. (Redding, CA, USA).

Samples were prepared by dissolving the lipids and also peptide in a 1:1 mixture of dichlormethane and methanol. Further, appropriate amounts of the solution were mixed together, dried in a weak nitrogen stream and kept under vacuum overnight in order to remove residual solvent. Aqueous lipid dispersions were prepared by weighing appropriate amounts of the lipid/lipid or lipid/peptide mixtures and of Milli-Q water into suitable flasks.

Samples for AFM experiments were prepared by direct fusion of small unilamellar vesicles (SUVs) on a piece of freshly cleaved mica. SUVs were obtained by sonication using a Sonifier Cell Disruptor B-15 (Branson, Germany) until the solution became completely transparent, ensuring mostly unilamellar vesicles. The samples were incubated for 20 min at room temperature and rinsed by exchanging ten times the lipid sample with 150 mM NaCl solution or with Milli-Q water. In doing so the mica-supported membrane was never allowed to dry. Sound velocity,

density and heat capacity measurements were performed using large unilamellar vesicle (LUV) suspensions. LUVs of uniform size were produced by extrusion [32] utilizing a Lipofast extruder (Avestin Inc., Ottawa, Canada) and polycarbonate filters with 100 nm pore size. During the extrusion procedure the sample temperature was always kept above T_m in order to facilitate the pushing of the vesicle suspension through the filter membrane. Right before use of the samples the extruded vesicle solutions were degassed for 15 min to remove air microbubbles.

AFM images of mica-supported membranes were recorded in both contact and tapping mode with the aid of a MultiMode instrument with NanoScope IIIa controller (Digital Instruments, Santa Barbara, CA, USA). Oxide-sharpened silicon nitride AFM probes (Digital Instruments) with nominal spring constants 0.06 and 0.12 N/m were used. The force was kept minimal during scanning by routinely decreasing it until the tip left the surface and subsequently increasing it slightly to just regain contact. The scan rate was 5 to 8 lines per second for the contact mode of operation and 1 to 3 lines per second for the tapping mode. All images with 512×512 pixels were analyzed with non-commercial software WSxM© (Nanotec Electronica, http://www.nanotec.es).

The sound velocity c of the sample has been measured at some MHz using three setups based on resonator methods. The liquid was contained in a small-volume cavity provided with piezoelectric transducers. One transducer was operated by a synthesized signal generator to set up a standing wave pattern in the cavity. Due to the multiple reflections of the waves the pathway of interactions between the acoustic field and the sample liquid was virtually increased by a significant factor. Along with the cell length the series of resonance frequencies in the transfer function of the cavity allowed for the calculation of the desired c. The effective cell length was obtained from calibration measurements with water, the sound velocity of which is well known [33]. We used two home-made apparatus. A single cavity resonator was operated in a manual mode by adjusting the frequency of the signal generator to match the frequency of a selected relative maximum in the transfer function of the cell. Also a twin cell was applied in which one cavity was filled with the sample liquid, the other one with water as reference [34]. Using this cell a computer controlled determination of the resonator transfer function was employed, followed by a regression analysis to determine the resonance frequency of the sample cell and the reference cell, respectively. Additionally, a commercial apparatus (HR-US 102, Ultrasonic Scientific Ltd., Dublin, Ireland) was applied, equipped with two 1 ml quartz cuvettes for the sample and the reference liquid, respectively [35]. A titration accessory of HR-US 102 spectrometer allowed stepwise additions of a titrant to the sample and the reference liquid (buffer). We added alamethicin that had been dissolved in ethanol to a DMPC vesicle suspension. The effect of ethanol on the lipid bilayer solution has been studied by separate scans.

With the single resonator cell and the commercial cuvette setup the temperature was maintained constant during measurements to better than 0.02 K by circulating water from an external thermostatic bath. With the home-made twin cell apparatus a Peltier control enabled temperature stability better than 0.003 K [34]. The resolution in the sound velocity measurements with home-made setups was $\Delta c/c=10^{-5}$ and $\Delta c/c=1.5\cdot10^{-7}$ with the commercial apparatus [36]. Repeated measurements of samples, including cleaning and refilling procedures, revealed an error in the sound velocity data smaller than $\Delta c/c=10^{-4}$ with the home-made setups and smaller than $\Delta c/c=10^{-6}$ with the HR-US 102 spectrometer. The overall error in c is, of course, not smaller than that of the reference (e.g. $\Delta c/c=10^{-5}$ for water [33]).

The density of the samples has been measured to within $\Delta\rho/\rho=5\cdot10^{-6}$ using a high-precision vibrating tube densitometer [37] with built-in reference oscillator and Peltier temperature control (Physica DMA 500, Anton Paar, Graz, Austria). The instrument was calibrated against doubly distilled, ultrafiltered, degassed water. The error in the temperature of measurement was 0.01 K. Heat capacities were recorded in an up-scan mode on a differential scanning calorimeter (VP-DSC, MicroCal, Northampton, MA, USA) at a scan rate of 2 K/h. A suitable baseline was subtracted from the thermograms.

3. Results and discussion

3.1. Membranes from one phospholipid

Fig. 2a shows an AFM height image of a DPPC bilayer spread on a freshly cleaved mica surface. As the image has

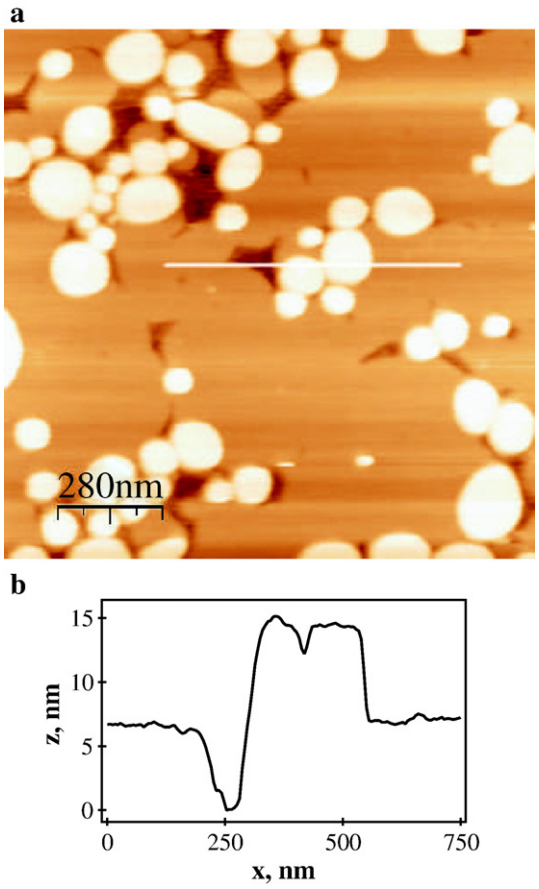

Fig. 2. 1.4×1.4 μm scan size height image of a mica-supported DPPC bilayer at room temperature (a) obtained by operating the AFM in the contact mode and (b) height profile along the white line of the height image.

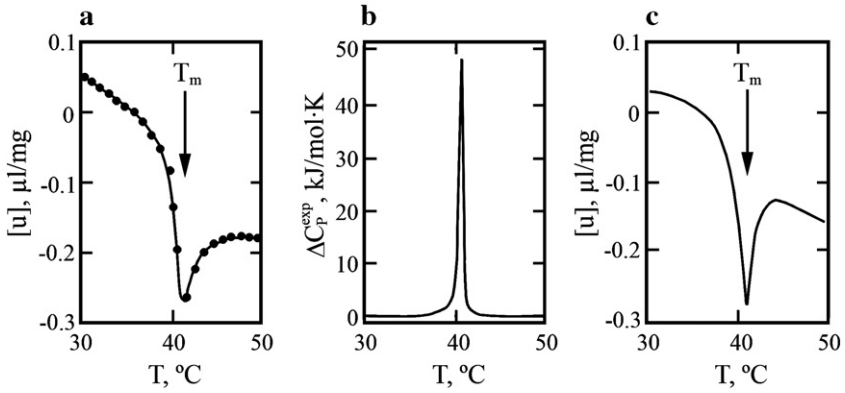

Fig. 3. Experimental sound velocity numbers (a), excess heat capacity (b), and sound velocity numbers as calculated using the c_P^{exc} curve (c) for a DPPC solution plotted versus temperature [50].

been taken at room temperature the bilayer was distinctly below the phase transition temperature T_m=41 °C. Dark regions in the height image correspond with the level of the mica, thus indicating membrane defects. Such parts of the mica surface which are not covered by lipid may result from an insufficient incubation time or from a too small lipid concentration. Bright regions in the image point at small pieces of a second bilayer, laying on the top of the first one. The height profile in part b of Fig. 2 yields the thickness of the first DPPC bilayer in the gel phase as 5 to 6 nm, in conformity with literature values of DPPC membranes [38,39]. The height difference between the upper surfaces of the second and the first bilayer amounts to 7 to 8 nm. The finding of a distance that is by about 2 nm larger than that between the upper surface of the first bilayer and the mica surface is taken an indication of a water layer between both membranes [40,41]. Between the dark and the bright spots the mica-supported DPPC membranes display a very flat surface in AFM images. The same is true for mica-supported DLPC membranes (T_m=−2.1 °C) which, at room temperature, are well above the main phase transition temperature.

In Fig. 3a sound velocity data of an aqueous suspension of vesicles from DPPC are shown as a function of temperature around T_m. In order to accentuate the effect of the membranes in c the sound velocity number, as defined by the equation [42]

$$[u] = (c - c_0)/\left(c_0\hat{C}\right), \tag{1}$$

is plotted in the diagram. In this equation c_0 denotes the sound velocity of the solvent water and $\hat{C}$ the solute concentration in mg/ml. Normalization of the data by $\hat{C}$ results in almost identical temperature scans from samples of different lipid concentration [43]. The sound velocity number displays an overall decrease with T and, in addition, a small relative minimum around the main phase transition temperature T_m. In the following we shall show that the sound velocity number and the heat capacity of membrane systems are correlated.

The sound velocity is related to the density ρ and the adiabatic compressibility κ_S according to the Newton–Laplace relation

$$c = (\rho\kappa_S)^{-1}. \tag{2}$$

As the apparent specific partial volume [44]

$$\chi_v = \rho_0^{-1} - [\rho] \tag{3}$$

exhibits a step-like change at T_m (Fig. 4a) the overall increase in the compressibility with T is superimposed by a relative maximum (Fig. 4b), reflecting the minimum in c. In Eq. (3) subscript "0" indicates again a quantity referring to the pure solvent and

$$[\rho] = (\rho - \rho_0)/\left(\rho_0\hat{C}\right) \tag{4}$$

is the density number. In Fig. 4b we likewise prefer a reduced quantity, namely the apparent specific adiabatic compressibility, defined by

$$\varphi_k = (\kappa_S V - \kappa_{s0} V_0)/\left(\kappa_{s0} V\hat{C}\right). \tag{5}$$

Similar to DMPC solutions [43] a relative maximum in φ_k emerges at the phase transition temperature, indicating an enhanced compressibility of the membranes due to intense

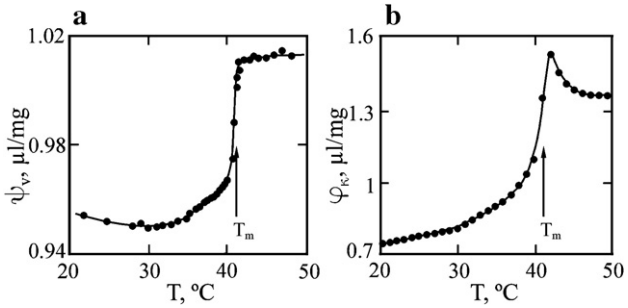

Fig. 4. Apparent specific partial lipid volume (a, [68]) and apparent specific adiabatic compressibility (b, [69]) for a DPPC vesicle solution displayed as a function of temperature.

fluctuations of their domain structure and of the lipid chain conformations.

Fig. 3b shows the excess heat capacity c_P^{exc} as obtained from the DSC experiments. The c_P^{exc} data exhibit a sharp maximum at the transition temperature, thus indicating a high degree of cooperativity in the phase transition of the DPPC membranes.

Based on the well-known thermodynamics relations between the heat capacity and the fluctuations in the enthalpy

$$c_P = \left(\overline{H}^2 - \overline{H}^2\right)/\left(RT^2\right) \tag{6}$$

as well as the isothermal compressibility κ_T and the fluctuations in the volume

$$\kappa_T = \left(\overline{V}^2 - \overline{V}^2\right)/\overline{V}RT \tag{7}$$

a theoretical relation between the isothermal compressibility and the excess heat capacity has been obtained [43,45]. In deriving this relation the enthalpy H^l of a hydrated lipid has been separated

$$\overline{H}^l(T) = \overline{H}_0^l(T) + \overline{\Delta H}^l(T) \tag{8}$$

into a bulk term $\overline{H}_0^l$, that is mainly due to bond vibrations and head group vibrations assumed to be independent of the melting process at T_m, and a differential term $\overline{\Delta H}^l$, representing the changes in chain isomerization and the change in dispersive interactions between chains. Correspondingly, the lipid volume is described by

$$\overline{V}^l(T) = \overline{V}_0^l(T) + \overline{\Delta V}^l(T). \tag{9}$$

Advantage is particularly taken from the experimental findings [46,47] that, close to the melting transition of the alkyl chains, $\overline{\Delta V}^l$ and $\overline{\Delta H}^l$ are almost perfectly proportional to each other

$$\overline{\Delta V}(T) = \gamma \cdot \overline{\Delta H}(T) \tag{10}$$

with a proportionality constant $\gamma = 7.8 \cdot 10^{-4}$ cm^3/J. This equation leads to a proportionality between the excess isothermal compressibility $\Delta\kappa_T$, linked to the fluctuations in the lipid state, and the heat capacity change Δc_P at the transition [43,45]. Additionally, the Maxwell relations yield the adiabatic compressibilities from Eq. (2) as a function of the isothermal compressibility Eq. (7) and the volume expansion coefficient

$$\kappa_S(T) = \kappa_S(T) - \frac{T}{\overline{V}c_P}\left(\frac{d\overline{V}}{dT}\right)^2. \tag{11}$$

Because of the finite time of heat exchange within the sample the heat capacity, in general, is a function of frequency. Volume perturbation calorimetry [48,49] and pressure jump calorimetry [14], however, have revealed a time constant on the second time scale for the heat exchange between the lipid phase and the solvent. Hence this heat exchange needs a significantly larger time than the period in the acoustical signal of the sound velocity measurements. Therefore both reservoirs, membranes and water, may be considered adiabatically decoupled and the adiabatic compressibility of the lipid suspensions can be considered the weighted average of the adiabatic compressibility of water and of the hydrated lipid

$$\kappa_S(T) = (1 - \upsilon_l)\kappa_w + \upsilon_l\kappa_l. \tag{12}$$

Here subscripts l and w denote the quantities for the lipid and the aqueous phase, respectively, and v_l is the volume fraction of the lipid membranes. The decoupling of the lipid membrane from the aqueous environment on the time scale of the ultrasonic experiment (~200 ns) implies that the heat generated upon compression is stored in the membrane itself and does not dissipate out into the aqueous medium. Thus, when describing the adiabatic compressibility of the lipids using Eq. (11) the heat capacity in this equation contains only contributions from the lipid but not from surrounding water. Although heat conduction in water is fast, the agreement of experiment with theory justifies the assumption [43,45,50]. We therefore consider the thermal decoupling of lipids and membranes as a result of our previous analysis and also of the present data (see below, Fig. 5). It would be interesting to obtain a more detailed understanding of the origin of such a decoupling in future research.

The sound velocity number profile resulting from the c_P^{exc} scan (Fig. 3b) of the DPPC suspension is displayed in Fig. 3c. Calculating the $[u]$ values linear relationships

$$\kappa_{T,a}^l = \kappa_{0,a} + \Delta\kappa_a(T - 303.15\text{K}) \tag{13}$$

have been assumed to adequately represent the temperature dependence in the background compressibility of the membranes in the gel (a=gel) and fluid (a=fluid) state, respectively. Parameters $\kappa_{0,a}$ and $\Delta\kappa_a$ have been adjusted to model the baseline in the experimental sound velocity profiles. The curve in Fig. 3c resulting thereby nicely agrees with the experimental data (Fig. 3a). Hence, in correspondence with previous results [43,45], not just the absolute $[u]$ values but also the shape in the temperature dependence of the sound velocity numbers are correctly predicted by theory.

3.2. Membranes from binary lipid mixtures

Membranes from DLPC and DPPC reveal a broad range in which gel and lipid domains coexist [51]. Comparison of

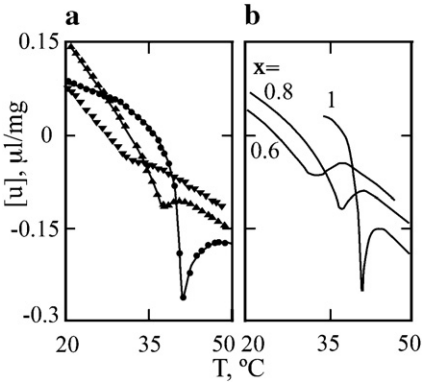

Fig. 5. (a) Measured sound velocity numbers $[u]$ and (b) $[u]$ profiles as calculated from the c_P^{exc} data in [50] for DLPC/DPPC mixtures with mole fraction × of DPPC (●, x=1; ▲, x=0.8; ▼, x=0.6 [50]).

experimental sound velocity numbers for such numbers to those calculated from c_P^{exc} scans (Fig. 5) demonstrates the applicability of the theoretical model also for lipid mixtures.

At some DLPC/DPPC molar ratios AFM images of mica-supported two-component bilayers have been taken. A height image at mole fraction $x=0.67$ of DPPC is shown in Fig. 6a. Black regions correspond to the mica surface. The elongated bright region in the middle of the section indicates a second bilayer on the top of the first one. The first bilayer demonstrates the existence of at least three types of domains with different height scales, further on referred to as I, II and III domains, respectively. The height differences are revealed by the cross sectional profile in Fig. 6b. The height difference between I and II domains amounts to approximately 0.9 nm. Between type II and type III domains an additional difference of about 0.6 nm exists. Lipid II domains with lateral dimensions in the micrometer range predominate. Both other types, with sizes between tens and hundreds of nanometers, are randomly distributed over the type II domains.

The height image of another part of the same DLPC/DPPC sample (Fig. 7a) indicates again type I and type III domains embedded in the larger type II domains. Interestingly, the corresponding phase image (Fig. 7b) does not distinguish between I and II domains. No final agreement exists on how to interpret phase images. Clearly, the viscoelastic properties of the material plays a role.

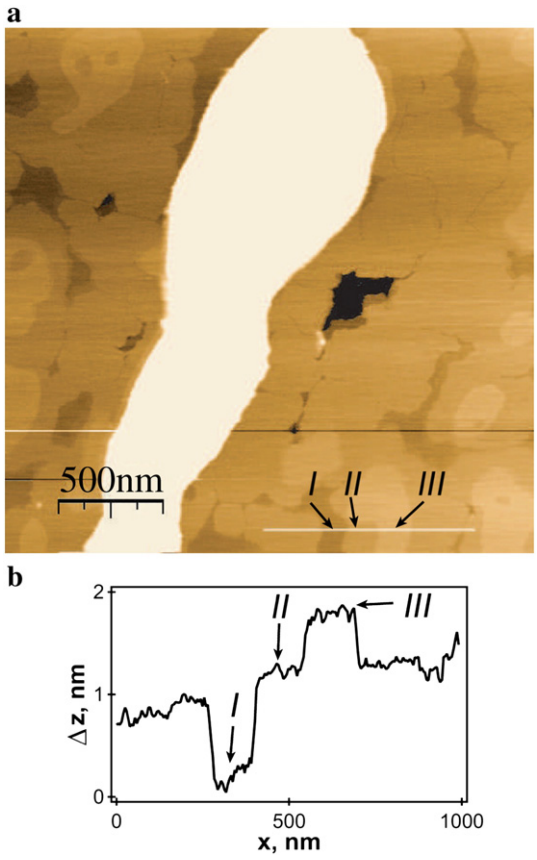

Fig. 6. (a) 2.5×2.5 μm scan size height image of a mica-supported DLPC/DPPC bilayer at 22 °C (mole fraction of DPPC $x=0.67$l obtained by operating the AFM in the tapping mode and (b) height difference profile along the white line of the height image.

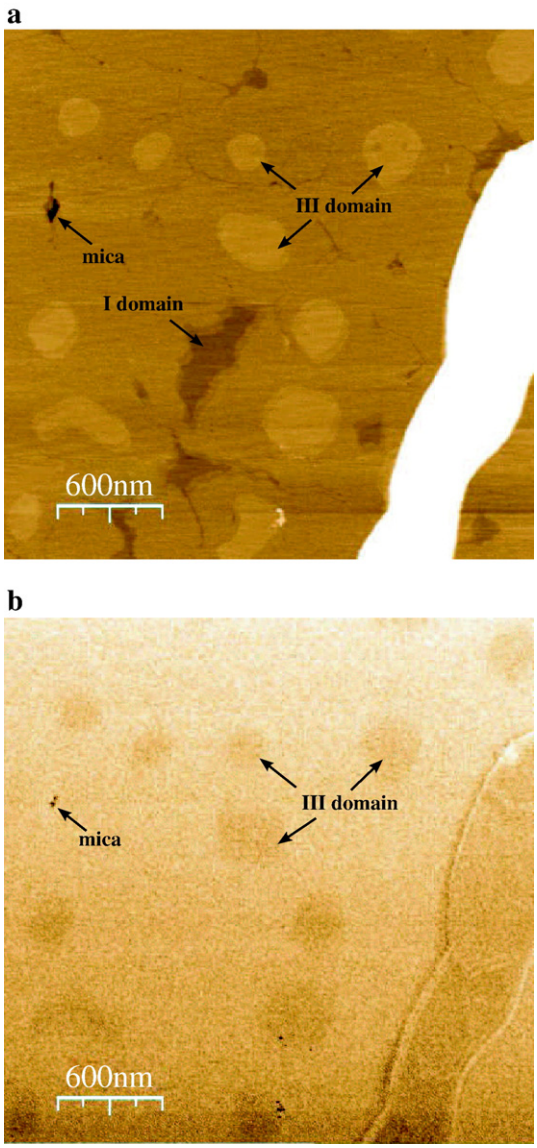

Fig. 7. 2.5×2.5 μm AFM scans of the DLPC/DPPC bilayer of Fig. 6: (a) height, (b) phase image.

In principle, adhesion effects can also have an effect, but we do not see any reason to assume that adhesion to the cantilever tip is different in the different phases of neutral phospholipids. It seems likely that larger phase contrast in the present case indicates softer material. The lipid domain with largest thickness (type III) are stiffer than both domain types with lower height. Obviously, the elastic properties of I and II domains are rather identical.

According to Gibbs' phase rule one expects up to two coexisting phases in a phase diagram at constant pressure and excess water (the possibility of three-component coexistence exists only at single eutectic or peritectic points). However, these considerations apply only to macroscopic phase separation where domain boundaries can be ignored. Whether the domains in our recordings are in fact phases (meaning that the

phase rule can be applied) is unclear. Further, in the presence of alamethicin one has a three-component system that allows for three coexisting phases (or even four at individual points of the phase diagram). There is also the possibility that the mica surface influences the appearance of the bilayers.

3.3. Alamethicin-containing membranes

The series of diagrams in Fig. 8 show that, for DMPC as well as DPPC bilayers with 1 and 2 mol% alamethicin added, respectively, the sound velocity numbers of the peptide-containing membranes can be well calculated from the heat capacities, assuming again the change in volume and the excess enthalpy of the lipid proportional to each other Eq. (10). In the c_P-properties of the DMPC membranes, like in LUV suspensions from pure DMPC [52], a splitting of the transition peak is found. In correspondence to the behavior of DMPG [53] this splitting is believed to result from changes in the vesicle geometry occurring in the lipid melting region. DPPC LUV suspensions indicate such splitting only at the higher alamethicin content. The heat capacity profiles in the presence of alamethicin are hardly shifted as compared to the pure lipid. This indicates that the protein does not partition well in both gel and fluid phase. This is indicative for situations where the proteins either accumulate at domain or at pore interfaces [54]. Since minor shifts to lower temperatures are observed this indicates that the partitioning is slightly better in the fluid phase.

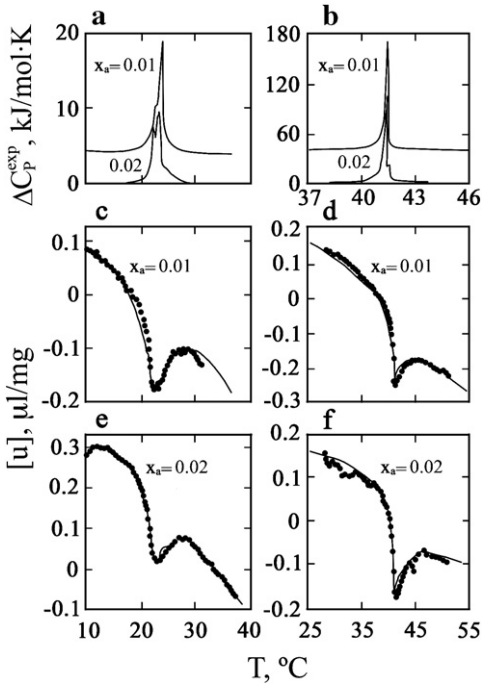

Fig. 8. Heat capacity traces for large unilamellar vesicle suspensions from DMPC (a) and DPPC (b) with 1 and 2 mol% alamethicin added, respectively, as well as sound velocity number profiles for the same suspensions (c and e refer to DMPC, d and f to DPPC). The lipid concentration is 5 µmol/l. For a clearer data representation the heat capacity curves were shifted for a constant offset along the c_P^{exc} axis.

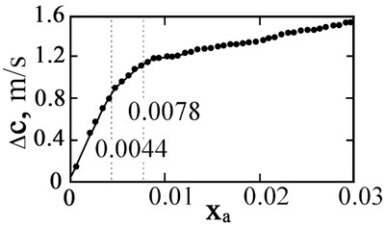

Fig. 9. Titration curve for a DMPC suspension with lipid concentration 7.538 µmol/l: sound velocity difference $\Delta c = c - c_{ref}$ as a function of mole fraction x_a of alamethicin at 17.24 °C. Here c_{ref} is the sound velocity of the reference sample without alamethicin.

One may conclude from this that alamethicin rather forms pores within the fluid phase domains.

The sound velocity of the vesicle suspensions reveals an interesting behavior on continuous addition of alamethicin, as shown for a DMPC sample in Fig. 9. The sound velocity change Δc caused by the peptide defines three concentration ranges. At an alamethicin mole fraction x_a smaller than $4.4 \cdot 10^{-3}$ the slope of $d\Delta c/dx_a$ is as high as 200 m/s, at $4.4 \cdot 10^{-3} \leqslant x_a < 7.8 \cdot 10^{-3}$ the slope $d\Delta c/dx_a = 65$ m/s follows and at higher peptide content $d\Delta c/dx_a = 18$ m/s. At low alamethicin content ($x_a < 4.4 \cdot 10^{-3}$) the helical peptide molecules are adsorbed to the lipid bilayer

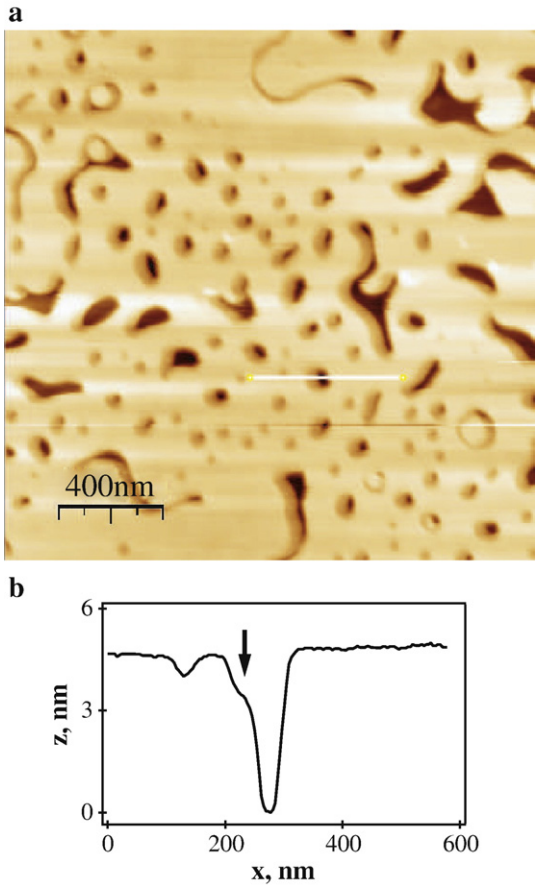

Fig. 10. 2×2 µm AFM height image of a mica-supported DPPC bilayer containing alamethicin ($x_a = 0.01$) at room temperature (a) and height profile along the white line of the height image (b). The arrow marks the height of the shell near the alamethicin pores.

membrane–water interface [55–58]. Molecular dynamics simulations show that the alamethicin helix structure is stabilized by the peptide interactions with the lipid polar head groups [56] and also by the more favorable hydration properties of alamethicin in its surface binding state. As the density of the DMPC suspension remains almost constant on addition of alamethicin, the significant increase of Δc with x_a (Fig. 9) reflects a decrease of the adiabatic compressibility κ_S Eq. (2), which may result from two effects. The peptide–membrane interactions are accompanied by a local deformation of the membrane [55,59] and a lateral shift of lipid molecules. The internal tension of the membrane is enhanced thereby [60,61], thus reducing the compressibility. Additionally, the formation of a hydration layer around alamethicin helices adsorbed to the membrane surface may reduce κ_S.

The second concentration range ($4.4 \cdot 10^{-3} \leqslant x_a \leqslant 7.8 \cdot 10^{-3}$) is assigned to the transition region in which, due to the finite diameter of the membrane deformations, no further peptides may be adsorbed at the bilayer–water interface and more and more alamethicin molecules are inserted into the bilayers. The minimum in the free energy is reached by a subtle balance between the concentration of adsorbed and of inserted peptides. The insertion of alamethicin results in a stabilization of the membranes and thus in a reduction of the compressibility. At high alamethicin content ($x_a \geq 7.8 \geq 10^{-3}$) no more peptide is adsorbed on the bilayer surface. Rather all additional alamethicin molecules are inserted in the membranes where they cluster to form pores.

Insertion of alamethicin causes membrane thinning [62]. The energy cost of membrane thinning raises the free energy of the alamethicin interactions with the membrane–water interface [63]. Fig. 10a presents an AFM image of an alamethicin-containing DPPC membrane at room temperature. Dark regions show the peptide-induced defects (”holes”) in the bilayer. The holes are surrounded by an area with reduced membrane height, appearing darker than the undisturbed lipid bilayer regions. The height profile across a hole (Fig. 10b) reveals the reduced height in the 3 to 4 nm range whereas the thickness of the undisturbed bilayer amounts to 5–6 nm. The latter value agrees well with the generally accepted thickness of DPPC bilayers in the gel phase [38,39,45], whereas the height of the shell region corresponds with the thickness of DPPC membranes in the fluid phase. As symmetric height profiles with reduced membrane thickness on both sides of the hole have been also found, it has been concluded that the reduced height around the holes reflects nanoscopic lipid domains in the fluid phase [52] which form in the gel phase membrane to reduce the structural mismatch between the alamethicin helices, with about 3.5 nm length, and the thickness of the DPPC bilayer. Though the areas with reduced height are not homogeneously distributed around all holes but appear sometimes on one side of a defect only (Fig. 10), it has been argued that these areas unlikely reflect experimental artifacts but rather indicate alamethicin-induced fluid DPPC domains which, in phase images, show up as regions softer than the undisturbed membrane [52].

4. Conclusions

The purpose of the present paper was to demonstrate the coupling between the susceptibilities of the membrane system (i.e. of compressibility and heat capacity) with the lateral arrangement of peptides and lipids in different physical states. In particular, the insertion of the pore-forming peptide alamethicin into membranes leads to a rearrangement of domains and lipids. It results in altered compressibility and increased likelihood of fluid lipids close to the peptide pore interfaces.

Although only one particular peptide (alamethicin) was studied here the implications are of rather general nature. They can be summarized as follows: When peptides or proteins influence the heat capacity profiles of membranes they must influence the distribution of lipids with different state or chemical nature. As a necessity they will influence the elastic constants in their environment [52] when the membrane system is close to a melting transition. In the light of the experimental fact that many biological membranes are situated slightly above such a melting transition [64] this suggests an important role of such processes in controlling the physical features of lipid–protein complexes in native biological membranes.

Acknowledgements

We are indebted to Professor T. Bjørnholm, University of Copenhagen, for making atomic force microscopes of the Nano-Science Center available for this study. Financial support from the graduate school ”Neuronal Signalling and Cellular Biophysics” at the Georg-August-University, Göttingen, is gratefully acknowledged.

References

[1] R.B. Gennis, Biomembranes: Molecular Structure and Function, 1989.
[2] R. Lipowsky, E. Sackmann, Structure and Dynamics of Membranes, vol. 1A, 1995.
[3] R. Zhang, W. Sun, S. Tristram-Nagle, R.L. Headrick, R.M. Suter, J.F. Nagle, Critical fluctuations in membranes, Phys. Rev. Lett. 74 (1995) 2832.
[4] O.G. Mouritsen, K. Jorgensen, Micro-, nano- and meso-scale heterogeneity of lipid bilayers and its influence on macroscopic membrane properties, Mol. Membr. Biol. 12 (1995) 15–20.
[5] S.L. Veatch, O. Soubias, S.L. Keller, K. Gawrisch, Critical fluctuations in domain-forming lipid mixtures, PNAS 104 (2007) 17650–176505.
[6] O.G. Mouritsen, K. Jorgensen, Small-scale lipid–membrane structure: simulation versus experiment, Curr. Opin. Struct. Biol. 7 (1997) 518–527.
[7] T. Heimburg, A model for the lipid pretransition: coupling of ripple formation with the chain-melting transition, Biophys. J. 78 (2000) 1154–1165.
[8] O.G. Mouritsen, K. Jorgensen, Dynamical order and disorder in lipid bilayers, Chem. Phys. Lipids 73 (1994) 3–25.
[9] S. Halstenberg, W. Schrader, P. Das, J.K. Bhattacharjee, U. Kaatze, Critical fluctuations in the domain structure of lipid membranes, J. Chem. Phys. 118 (2003) 5683–5691.
[10] W. Schrader, S. Halstenberg, R. Behrends, U. Kaatze, Critical slowing in lipid bilayers, J. Phys. Chem. B 107 (2003) 14457–14463.
[11] L.P. Kadanoff, J. Swift, Transport coefficients near the liquid–gas critical point, Phys. Rev. 166 (1968) 89–101.
[12] B.I. Halperin, P.C. Hohenberg, Scaling laws for dynamic critical phenomena, Phys. Rev. 177 (1969) 952–971.
[13] R.A. Ferrell, Decoupled-mode dynamical scaling theory of the binary-liquid phase transition, Phys. Rev. Lett. 24 (1970) 1169–1172.
[14] P. Grabitz, V.P. Ivanova, T. Heimburg, Relaxation kinetics of lipid membranes and its relation to the heat capacity, Biophys. J. 82 (2002) 299–309.
[15] H.M. Seeger, M.L. Gudmundsson, T. Heimburg, How anesthetics, neurotransmitters, and antibiotics influence the relaxation processes in lipid membranes, J. Phys. Chem. B 111 (2007) 13858–13866.

[16] D.S. Cafiso, Alamethicin: a peptide model for voltage gating and protein–membrane interactions, Annu. Rev. Biophys. Biomol. Struct. 23 (1994) 141–165.
[17] T. Salditt, C. Li, A. Spaar, Structure of antimicrobial peptides and lipid membranes probed by interface-sensitive X-ray scattering, Biochim. Biophys. Acta 1758 (2006) 1483–1498.
[18] R.O. Fox, F.M. Richards, A voltage gated ion channel inferred from the crystal structure of alamethicin at 1.5 Å resolution, Nature 300 (1982) 325–330.
[19] G. Boheim, Statistical analysis of alamethicin channels in black lipid membranes, J. Membr. Biol. 19 (1974) 277–303.
[20] J.E. Hall, Voltage-dependent lipid flip-flop induced by alamethicin, Biophys. J. 33 (1981) 373–381.
[21] G. Schwarz, P. Savko, Structural and dipolar properties of the voltage-dependent pore former alamethicin in octanol/dioxane, Biophys. J. 39 (1982) 211–219.
[22] I. Vodyanoy, J.E. Hall, T.M. Balasubramanian, Alamethicin-induced current–voltage curve asymmetry in lipid bilayers, Biophys. J. 42 (1983) 71–82.
[23] V.M. Aguilella, S.M. Bezrukov, Alamethicin channel conductance modified by lipid charge, Eur Biophys J 30 (2001) 233–241.
[24] M. Eisenberg, J. Hal, C. Mead, The nature of the voltage-dependent conductance induced by alamethicin in black lipid membranes, J. Membr. Biol. 14 (1973) 143–176.
[25] W. Hanke, G. Boheim, The lowest conductance state of the alamethicin pore, Biochim. Biophys. Acta 596 (1980) 456–462.
[26] S.L. Keller, S.M. Bezrukov, S.M. Gruner, M.W. Tate, I. Vodyanoy, V.A. Parsegian, Probability of alamethicin conductance states varies with nonlamellar tendency of bilayer phospholipids, Biophys. J. 65 (1993) 23–27.
[27] K. He, S. Ludtke, D. Worcester, H. Huang, Neutron scattering in the plane of membranes: structure of alamethicin pores, Biophys. J. 70 (1996) 2659–2666.
[28] R. Cantor, Size distribution of barrel-stave aggregates of membrane peptides: influence of the bilayer lateral pressure profile, Biophys. J. 82 (2002) 2520–2525.
[29] Y.P. Zhang, R.N. Lewis, R.S. Hodges, R.N. McElhaney, Peptide models of helical hydrophobic transmembrane segments of membrane proteins. 2. Differential scanning calorimetric and FTIR spectroscopic studies of the interaction of ac-k2-(la)12-k2-amide with phosphatidylcholine bilayers, Biochemistry 34 (1995) 2362–2371.
[30] O.G. Mouritsen, M. Bloom, Models of lipid–protein interactions in membranes, Annu. Rev. Biophys. Biomol. Struct. 22 (1993) 145–171.
[31] M.Ø. Jensen, O.G. Mouritsen, Lipids do influence protein function — the hydrophobic matching hypothesis revisited, Biochim. Biophys. Acta 1666 (2004) 205–226.
[32] R.C. MacDonald, R.I. MacDonald, B.P.M. Menco, K. Takeshita, N.K. Subbarao, L. Hu, Small-volume extrusion apparatus for preparation of large, unilamellar vesicles, Biochim. Biophys. Acta 1061 (1991) 297–303.
[33] N. Bilaniuk, G.S.K. Wong, Speed of sound in pure water as a function of temperature, J. Acoust. Soc. Am. 93 (1993) 1609–1612.
[34] K. Lautscham, F. Wente, W. Schrader, U. Kaatze, High resolution and small volume automatic ultrasonic velocimeter for liquids, Meas. Sci. Technol. 11 (2000) 1432–1439.
[35] V. Buckin, C. Smyth, High-resolution ultrasonic resonator measurements for analysis of liquids, Seminars in food analysis 4 (1999) 113–130.
[36] C. Dwyer, L. Donnelly, V. Buckin, Ultrasonic analysis of rennet-induced pre-gelation and gelation processes in milk, J. Dairy Res. 72 (2005) 303–310.
[37] O. Kratky, H. Leopold, H. Stabinger, Dichtemessung an Fluessigkeiten und Gasen auf 10^{-6} g/cm^3 bei 0,6 cm^3 Probenvolumen, Z. angew. Physik 27 (1969) 273–277.
[38] L.K. Tamm, H.M. McConnell, Supported phospholipid bilayers, Biophys. J. 47 (1985) 105–113.
[39] J. Mou, J. Yang, Z. Shao, Tris(hydroxymethyl)aminomethane (c4h11no3) induced a ripple phase in supported unilamellar phospholipid bilayers, Biochemistry 33 (1994) 4439–4443.
[40] J.F. Nagle, Theory of the main lipid bilayer phase transition, Ann. Rev. Phys. Chem. 31 (1980) 157–195.
[41] L. Makowski, J. Li, Topics in Molecular and Structural Biology: Biomembrane Structure and Function, 1984, pp. 43–166.
[42] A.P. Sarvazyan, T.V. Chalikian, Theoretical analysis of an ultrasonic interferometer for precise measurements at high pressures, Ultrasonics 29 (1991) 119–124.
[43] S. Halstenberg, T. Heimburg, T. Hianik, U. Kaatze, R. Krivanek, Cholesterol-induced variations in the volume and enthalpy fluctuations of lipid bilayers, Biophys. J. 75 (1998) 264–271.
[44] N. Taulier, T.V. Chalikian, Compressibility of protein transitions, Biochim. Biophys. Acta 1595 (2002) 48–70.
[45] T. Heimburg, Mechanical aspects of membrane thermodynamics. Estimation of the mechanical properties of lipid membranes close to the chain melting transition from calorimetry, Biochim. Biophys. Acta 1415 (1998) 147–162.
[46] F.H. Anthony, R.L. Biltonen, E. Freire, Modification of a vibrating-tube density meter for precise temperature scanning, Anal. Biochem. 116 (1981) 161–167.
[47] H. Ebel, P. Grabitz, T. Heimburg, Enthalpy and volume changes in lipid membranes. I. The proportionality of heat and volume changes in the lipid melting transition and its implication for the elastic constants, J. Phys. Chem. B 105 (2001) 7353–7360.
[48] W.W.V. Osdol, R.L. Biltonen, M.L. Johnson, Measuring the kinetics of membrane phase transitions, J. Biochem. Biophys. Methods 20 (1989) 1–46.
[49] W.W. van Osdol, M.L. Johnson, Q. Ye, R. Biltonen, Relaxation dynamics of the gel to liquid-crystalline transition of phosphatidylcholine bilayers. Effects of chainlength and vesicle size, Biophys. J. 59 (1991) 775–785.
[50] W. Schrader, H. Ebel, P. Grabitz, E. Hanke, T. Heimburg, M. Hoeckel, M. Kahle, F. Wente, U. Kaatze, Compressibility of lipid mixtures studied by calorimetry and ultrasonic velocity measurements, J. Phys. Chem. B 106 (2002) 6581–6586.
[51] H. Seeger, M. Fidorra, T. Heimburg, Domain size and fluctuations at domain interfaces in lipid mixtures, Macromol. Symp. 219 (2005) 85–96.
[52] V. Oliynyk, U. Kaatze, T. Heimburg, Defect formation of lytic peptides in lipid membranes and their influence on the thermodynamic properties of the pore environment, Biochim. Biophys. Acta 1768 (2007) 236–245.
[53] M.F. Schneider, D. Marsh, W. Jahn, B. Kloesgen, T. Heimburg, Network formation of lipid membranes: triggering structural transitions by chain melting, Proc. Natl. Acad. Sci. U. S. A. 96 (1999) 14312–14317.
[54] V.P. Ivanova, I.M. Makarov, T.E. Schäffer, T. Heimburg, Analyzing heat capacity profiles of peptide-containing membranes: cluster formation of gramicidin A. Biophys. J. 84 (2003) 2427–2439.
[55] K. He, S. Ludtke, W. Heller, H. Huang, Mechanism of alamethicin insertion into lipid bilayers, Biophys. J. 71 (1996) 2669–2679.
[56] D.P. Tieleman, H.J. Berendsen, M.S. Sansom, Surface binding of alamethicin stabilizes its helical structure: molecular dynamics simulations, Biophys. J. 76 (1999) 3186–3191.
[57] M.J. Zuckermann, T. Heimburg, Insertion and pore formation driven by adsorption of proteins onto lipid bilayer membrane–water interfaces, Biophys. J. 81 (2001) 2458–2472.
[58] F.-Y. Chen, M.-T. Lee, H.W. Huang, Evidence for membrane thinning effect as the mechanism for peptide-induced pore formation, Biophys. J. 84 (2003) 3751–3758.
[59] W.T. Heller, K. He, S.J. Ludtke, T.A. Harroun, H.W. Huang, Effect of changing the size of lipid headgroup on peptide insertion into membranes, Biophys. J. 73 (1997) 239–244.
[60] H. Isambert, Understanding the electroporation of cells and artificial bilayer membranes, Phys. Rev. Lett. 80 (1998) 3404.
[61] P. Sens, H. Isambert, Undulation instability of lipid membranes under an electric field, Phys. Rev. Lett. 88 (2002) 128102.
[62] F.-Y. Chen, M.-T. Lee, H.W. Huang, Sigmoidal concentration dependence of antimicrobial peptide activities: a case study on alamethicin, Biophys. J. 82 (2002) 908–914.
[63] H.W. Huang, Elasticity of lipid bilayer interacting with amphiphilic helical peptides, J. Phys. II France 5 (1995) 1427–1431.
[64] T. Heimburg, A.D. Jackson, On soliton propagation in biomembranes and nerves, Proc. Natl. Acad. Sci. USA 102 (2005) 9790–9795.

[65] J.K. Bhattacharjee, R.A. Ferrell, Dynamic scaling theory for the critical ultrasonic attenuation in a binary liquid, Phys. Rev. A 24 (1981) 1643–1646.
[66] R.A. Ferrell, J.K. Bhattacharjee, Dynamic scaling theory of the critical attenuation and dispersion of sound in a classical fluid: The binary liquid, Phys. Rev. A 31 (1985) 1788–1809.
[67] J.K. Bhattacharjee, R.A. Ferrell, Scaling theory of critical ultrasonics near the isotropic-to-nematic transition, Phys. Rev. E 56 (1997) 5549–5552.
[68] M. Höckel, Experimentelle Untersuchungen wässriger Lipid-Suspensionen mittels Ultraschallabsorptionsspektroskopie, Kalorimetrie und Densitometrie, Diploma thesis (1999).
[69] W. Schrader, Schallgeschwindigkeitsmessungen, Kalorimetrie sowie dielektrische und akustische Spektroskopie an wässrigen Phospholipid-suspensionen, Ph.D. thesis (2001).